

Journal of Biomedical Optics

BiomedicalOptics.SPIEDigitalLibrary.org

Biologically relevant photoacoustic imaging phantoms with tunable optical and acoustic properties

William C. Vogt
Congxian Jia
Keith A. Wear
Brian S. Garra
T. Joshua Pfefer

Biologically relevant photoacoustic imaging phantoms with tunable optical and acoustic properties

William C. Vogt, Congxian Jia, Keith A. Wear, Brian S. Garra, and T. Joshua Pfefer*

U.S. Food and Drug Administration, Center for Devices and Radiological Health, 10903 New Hampshire Avenue, Silver Spring, Maryland 20993, United States

Abstract. Established medical imaging technologies such as magnetic resonance imaging and computed tomography rely on well-validated tissue-simulating phantoms for standardized testing of device image quality. The availability of high-quality phantoms for optical-acoustic diagnostics such as photoacoustic tomography (PAT) will facilitate standardization and clinical translation of these emerging approaches. Materials used in prior PAT phantoms do not provide a suitable combination of long-term stability and realistic acoustic and optical properties. Therefore, we have investigated the use of custom polyvinyl chloride plastisol (PVCP) formulations for imaging phantoms and identified a dual-plasticizer approach that provides biologically relevant ranges of relevant properties. Speed of sound and acoustic attenuation were determined over a frequency range of 4 to 9 MHz and optical absorption and scattering over a wavelength range of 400 to 1100 nm. We present characterization of several PVCP formulations, including one designed to mimic breast tissue. This material is used to construct a phantom comprised of an array of cylindrical, hemoglobin-filled inclusions for evaluation of penetration depth. Measurements with a custom near-infrared PAT imager provide quantitative and qualitative comparisons of phantom and tissue images. Results indicate that our PVCP material is uniquely suitable for PAT system image quality evaluation and may provide a practical tool for device validation and intercomparison. © *The Authors. Published by SPIE under a Creative Commons Attribution 3.0 Unported License. Distribution or reproduction of this work in whole or in part requires full attribution of the original publication, including its DOI.* [DOI: [10.1117/1.JBO.21.10.101405](https://doi.org/10.1117/1.JBO.21.10.101405)]

Keywords: image quality; tissue phantoms; standardization; breast imaging; photoacoustic tomography; optoacoustics.

Paper 150784SSPR received Nov. 20, 2015; accepted for publication Jan. 15, 2016; published online Feb. 17, 2016.

1 Introduction

1.1 Photoacoustic Tomography

Photoacoustic tomography (PAT) is an emerging noninvasive imaging modality that combines pulsed or rapidly modulated optical irradiation with acoustic sensing to achieve greater penetration depths than pure optical imaging techniques.¹ While hemoglobin is the most significant endogenous chromophore for PAT, exogenous contrast agents such as bioconjugatable dyes^{2,3} or nanoparticles⁴ may also be used to enhance image contrast. Imaging applications reported in the literature include oximetry,⁵ lymph node detection,² and cancer detection, especially mammography.⁶

PAT systems reported in the literature show a wide variation in configuration, including sensor geometry, illumination geometry, optical wavelength, and acoustic frequency band. Many of these systems are also bimodal, capable of providing coregistered PAT and B-mode ultrasound imaging. Based on this variation in system operating parameters, a wide variation in device performance is expected. Standardized test methods and materials are needed in order to enable objective, quantitative characterization of PAT system performance. Phantom-based test methods are commonly used in medical imaging

device development and optimization, system intercomparison, benchmarking, clinical trial standardization, constancy testing, recalibration, quality assurance, and regulatory evaluation. For mature imaging technologies, such as magnetic resonance imaging, x-ray computed tomography, and ultrasound, tissue-simulating phantoms have been incorporated into international performance standards^{7,8} as well as accreditation programs.^{9,10} However, while there has been significant work on developing standardized phantoms for biophotonic imaging systems,^{11,12} no standardized phantom materials currently exist for photoacoustic imaging.

1.2 Review of Photoacoustic Phantom Materials

Development of appropriate phantom materials for evaluating photoacoustic imaging systems presents a challenge: phantoms should accurately mimic both the acoustic and optical properties of a particular tissue of interest. Phantom properties should also be independently tunable to enable the widest diversity in simulated tissue property sets. The most critical properties to control are optical absorption coefficient, optical scattering coefficient, speed of sound, and acoustic attenuation coefficient (Table 1 provides an approximate range of literature values for these properties in various tissues^{13–16}). In this study, we focus on simulating breast tissue properties, given the potential of PAT for mammography applications.^{6,17–21} Breast tissue may be thought of as a heterogeneous mixture of fatty and fibroglandular

*Address all correspondence to: T. Joshua Pfefer, E-mail: Joshua.Pfefer@fda.hhs.gov

Table 1 Optical and acoustic properties of representative soft tissues. Optical properties cover a spectrum from 600 to 900 nm, while acoustic properties span 1 to 10 MHz.

	Optical properties		Acoustic properties	
	Absorption coefficient (cm ⁻¹)	Reduced scattering coefficient (cm ⁻¹)	Speed of sound (m/s)	Acoustic attenuation coefficient (dB/cm)
General soft tissue	0.1–0.5	10–20	1450–1575	0.5–30
Breast fat	0.05–0.3	3–8	1430–1480	1–18
Breast parenchyma	0.1–0.3	5–15	1460–1520	2–25
Blood	2.0–10.0	10–15	~1560	0.1–2

tissues; fatty tissue has lower speed of sound and acoustic attenuation, while fibroglandular tissue has higher speed of sound and attenuation.²² Breast tissue composition and morphology are strongly affected by many factors, including age, menopausal state, and diseases such as cancer.²³ Thus, a highly tunable phantom material is needed to simulate the clinical range of breast compositions.

Many materials have been doped with optical absorbers and scatterers for use as optical phantoms, including hydrogels, paraffin, polymers, epoxies, and liquid fat emulsions such as Intralipid.¹¹ However, each of these materials has significant drawbacks for photoacoustic phantoms. Polymers and elastomers tend to have dissimilar speed of sound to tissue (e.g., silicone at 1030 m/s²⁴ or polydimethylsiloxane at 1300 m/s²⁵) while liquid fat emulsions possess low-acoustic attenuation, present a limited tuning range for speed of sound,²⁶ and degrade over time. Paraffin-based materials have been produced for ultrasound biopsy phantoms²⁷ and three-dimensional printed optical phantoms,²⁸ but it is unclear whether simultaneous optical and acoustic tuning can be achieved. Hydrogels such as agarose and gelatin containing hairs, absorbing inclusions, or fluid channels are commonly used for photoacoustic phantoms,^{17,29–34} but hydrogel material properties and overall gel mechanical strength typically destabilize quickly over a matter of days, making them ill-suited for long-term quality control or calibration phantoms. Another material that has seen considerable use in photoacoustics is poly(vinyl alcohol) (PVA) cryogel.^{18,30,35,36} PVA cryogels are formed through repeated freeze-thaw cycling, where each cycle simultaneously increases gel mechanical stiffness and optical turbidity without requiring light-scattering dopants. However, dye diffusion from inclusions has been observed after 1 year,¹⁸ and the acoustic and optical properties are not independently tunable, which may limit the types of tissues that can be accurately simulated.

Poly(vinyl chloride) plastisol (PVCP) is a suspension of a poly(vinyl chloride) (PVC) resin in liquid plasticizer. When heated to its fusion temperature (typically 170 to 190°C), the resin and plasticizer undergo mutual dissolution, resulting in gelation and fusion. After fusion, PVCP is poured into mold cavities to cool and solidify into arbitrary shapes. PVCP has been investigated as a material for photoacoustic phantoms,^{37–42} and solid PVCP inclusions within background PVCP matrix have been reported stable for at least six months,³⁸ suggesting that this material is suitable for fabricating highly robust phantoms with stable properties. The PVCP formulation reported in the literature is a commercial product for making soft fishing lures (M-F Manufacturing

Co., Inc., Fort Worth, Texas). This product, which produces translucent phantoms, can be doped with scatterers or absorbers to adjust the optical properties of resultant PVCP gels. However, this formulation has a speed of sound of ~1400 m/s,³⁷ which is lower than that of soft tissues (see Table 1). Additionally, the precise composition is proprietary, making product modification difficult. Fonseca et al. recently characterized the acoustic properties of PVCP, but found limited tunability of speed of sound.⁴³ Hungr et al. reported PVCP formulations with highly tunable speed of sound, but did not characterize PVCP acoustic attenuation.⁴⁴ Thus, adequate PVCP acoustic tunability has not been demonstrated. In this study, we present a tunable, nonproprietary PVCP formulation with adjustable acoustic and optical properties as a material for developing realistic tissue phantoms for optimizing and evaluating PAT systems.

1.3 Study Objectives

The purpose of this study is to advance realization of stable, biologically relevant phantoms for standardized assessment of PAT system performance based on well-validated test methods. Therefore, the primary study objectives were: (a) to evaluate the acoustic and optical properties of various PVCP formulations, (b) to assess the tunability and stability of PVCP optical and acoustic properties for an optimal formulation, and (c) to perform tissue-simulating phantom and *ex vivo* tissue measurements with a recently developed custom PAT system.

2 Methods

2.1 Plastisol Base Components and Additives

We first characterized gels made using commercially available PVCP (Super Soft Plastic, M-F Manufacturing Co.) to enable comparison between our custom PVCP materials and previously demonstrated PVCP phantoms. We also investigated the addition of a hardening agent (plastic hardener, M-F Manufacturing Co.) to modify the acoustic properties of commercial PVCP gels. In order to develop custom PVCP formulations, the base plastisol components must first be selected. For PVC resin, we selected Geon 121A, a dispersion-grade resin appropriate for making plastisols with high plasticizer content⁴⁵ (Mexichem Specialty Resins, Inc., Avon Lake, Ohio). From preliminary formulation and testing, we determined that plasticizer choice has a profound impact on both speed of sound and acoustic attenuation of PVCP gels. We performed acoustic characterization of 13 liquid plasticizers (Table 2), using methods described in Sec. 2.3, in order to identify

Table 2 Material properties and measured speed of sound of various plasticizers. Rows with bold font denote plasticizers further characterized in this study. Sound speed precision $< \pm 1$ m/s with 95% confidence. Molecular weight and density values provided by the supplier (Sigma-Aldrich, St Louis, Missouri).

Plasticizer	Speed of sound (m/s)	Molecular weight (g/mol)	Density (g/mL)
DEGB	1540	314.33	1.175
BBP	1511	312.36	1.100
DPGB	1480	342.39	1.120
Dimethyl phthalate	1469	194.18	1.190
Diethyl phthalate	1426	222.24	1.120
Diisononyl phthalate	1421	418.61	0.972
Bis[2-(2-butoxyethoxy)ethyl] adipate	1420	434.56	1.010
Dibutyl phthalate	1413	278.34	1.043
Trioctyl trimellitate	1413	546.78	0.990
Dimethyl adipate	1402	174.19	1.062
Diisobutyl phthalate	1386	278.34	1.039
DEHA	1381	370.57	0.925
Dibutyl adipate	1354	258.35	0.962

those plasticizers expected to produce tissue-relevant PVCP gels. From these 13 plasticizers, 4 were selected, based on speed of sound, for fabricating and characterizing PVCP gels: diethylene glycol dibenzoate (DEGB), dipropylene glycol dibenzoate (DPGB), benzyl butyl phthalate (BBP), and di(2-ethylhexyl) adipate (DEHA). For each plasticizer, PVCP gels were fabricated using PVC resin content of 10, 15, or 20% m/m. Gels were also prepared using binary mixtures of either DEGB/DPGB or BBP/DEHA, varying composition from 0 to 100% v/v of each plasticizer. All gels comprised of binary plasticizer mixtures contained 10% m/m PVC. Gel acoustic properties were characterized (see Sec. 2.3) and compared with measured acoustic properties of commercial PVCP gels.

Previous studies by others have demonstrated that optical scattering can be induced by TiO_2 in PVCP, while optical absorption can be increased by a black plastic colorant (BPC) consisting of carbon black dissolved in plasticizer (BPC, M-F Manufacturing Co.).^{37,38} In this study we also chose to utilize these additives. Optical scattering affects the penetration depth of PAT, while optical absorption can be used to increase background optical attenuation or to fabricate absorptive inclusions within the phantom. Acoustic attenuation is a combination of acoustic absorption and scattering losses. The gel structure typically imparts some base absorption and scattering, while scattering may be further increased by adding microparticles such as silica.^{29,46} We chose to impart acoustic scattering by adding soda lime glass microspheres (diameter = 38 to 63 μm , Spheriglass A, Potter Industries LLC, Malvern, Pennsylvania). Each additive was separately characterized in PVCP gels containing various concentrations of either 0 to 1% v/v BPC, 0 to 2 mg/mL TiO_2 , or 0 to 200 mg/mL glass microspheres. All gels used for

additive characterization were fabricated using a base PVCP mixture of 75%/25% v/v BBP/DEHA, 10% m/m PVC. Gel acoustic and optical properties were characterized using methods described in Secs. 2.3 and 2.5. Additionally, acoustic backscatter of gels containing glass microspheres was estimated using ultrasound B-mode imaging against a reference breast phantom (Sec. 2.4).

2.2 Phantom Fabrication

For each batch of phantoms, a stock PVCP solution was prepared by mixing either a plasticizer or binary mixture of plasticizers with 1% v/v calcium-zinc heat stabilizer (M-F Manufacturing Co.). PVC resin was then added and dissolved using magnetic stirring for 30 min, after which the solution was degassed for 60 min. At this point, the desired set of additives may be introduced to the stock solution. After mixing the PVC solution, TiO_2 was added to a 40 mL volume of stock solution, which was sonicated at 40°C for 30 min. This volume was then reintroduced to the stock solution and stirred for 5 min. At this point, BPC and/or glass microspheres may be added and stirred in for 5 min. PVCP formulations were heated following the method described by Bohndiek et al.³⁸ Briefly, PVCP was poured into a 100 mL round bottom flask in a magnetically-stirred oil bath maintained at 190°C using a thermocouple. The flask, which contained a stir bar, was then evacuated and stirred at ~300 rpm. Depending on composition, after about 3 to 5 min, the PVCP underwent a transition into a highly viscous state as gelation began; during this time the stir rate was reduced to ~75 rpm. After an additional 4 to 6 min, the PVCP approached full fusion, reducing viscosity and allowing stirring at initial speeds. At 12 to 15 min total heating time, the PVCP was poured into lubricated aluminum molds and cast into 5-mm thick, 38-mm diameter disks. All subsequent characterization experiments used PVCP phantoms in this shape, but with varied composition.

2.3 Acoustic Characterization

PVCP phantom acoustic properties were characterized using a broadband through-transmission technique.^{47,48} Briefly, PVCP disks of various compositions were placed in a water bath at the shared focus of a pair of coaxially aligned broadband transducers (V320, Panametrics, Waltham, Massachusetts), with one transducer acting as an emitter and the other as a detector. Both transducers had 7.5 MHz center frequencies, 1.27 cm diameters, and 3.81 cm focal lengths. Transducers were connected to a pulser/receiver (Model 5800PR, Panametrics), and received US signals were digitized (8 bit, 50 MHz) using a 400-MHz oscilloscope (9310C, Teledyne LeCroy, Chestnut Ridge, New York). Speed of sound in liquid plasticizers was also measured using this technique by replacing the solid sample mount with a liquid sample housing with thin plastic membranes. Because the membranes were thick enough to cause reverberation artifacts at higher acoustic frequencies, liquids were measured using a pair of lower-frequency transducers with 1 MHz center frequencies, 1.91 cm diameters, and 3.81 cm focal lengths (V314, Panametrics). The use of lower frequencies is valid because speed of sound is expected to have weak dependence on frequency (i.e., dispersion).⁴³ Additionally, attenuation of liquid plasticizers was not calculated, as attenuation was expected to be low and to not correspond to that of PVCP gels. Speed of sound in the sample, c_s , was calculated as⁴⁸

$$c_s = \frac{c_w}{1 + \frac{\Delta t}{\Delta x} c_w}, \quad (1)$$

where c_w is the speed of sound in water, Δt is the pulse delay between sample measurement and a water-only path reference measurement, and Δx is the sample thickness. The acoustic attenuation coefficient versus frequency, $\alpha(f)$, was calculated over 4 to 9 MHz as⁴⁷

$$\alpha(f) = \frac{10}{\Delta x} \log \left(\frac{P_w(f)}{P_s(f)} \right), \quad (2)$$

where $P_w(f)$ is the acoustic power spectrum measured through a water path, and $P_s(f)$ is the power spectrum measured through the sample. The range of 4 to 9 MHz was selected based on transducer frequency response and correlates to acoustic frequencies used in many reported PAT systems. Sample power spectra were acquired at three spatial positions in the sample, averaging 60 measurements at each position. Acoustic attenuation spectra are often assumed to follow a power-law form,¹⁴ for each of the three locations, the averaged attenuation spectrum was calculated and then fitted to the power-law relationship $\alpha(f) = af^n$, where a and n are fitting parameters. Mean and standard deviation were calculated for the set of three fitted attenuation spectra per sample, from which coefficient of variation was computed and expressed as a percentage.

2.4 Acoustic Backscatter Estimation

Since many PAT systems also provide ultrasound imaging, PVCP phantoms should provide tissue-relevant ultrasound images. Acoustic backscattering is the major source of contrast in ultrasound images; to characterize the effect of glass microspheres on acoustic backscattering and phantom ultrasound visualization, PVCP gels containing 0 to 200 mg/mL glass microspheres were placed over a commercial, breast-equivalent ultrasound phantom (Model 059, CIRS, Inc., Norfolk, Virginia) and imaged using the ultrasound mode in our custom PAT system (Sec. 2.7). This commercial phantom served as an approximate reference material for breast tissue echogenicity. A region of interest (ROI) was drawn over each PVCP gel, and pixel intensity was averaged and compared with that in the same ROI in the commercial breast phantom without an overlying PVCP sample.

2.5 Optical Characterization

PVCP optical properties were characterized using spectrophotometry. PVCP disks were placed between 1-mm thick, 75 mm × 50 mm glass slides (refractive index = 1.51) and diffuse transmittance and reflectance measurements were made over 400 to 1100 nm using an integrating sphere spectrophotometer (Lambda 1050, PerkinElmer, Waltham, Massachusetts). NIST-traceable Spectralon standards were used to normalize measurements. Liquid plasticizer absorption was also characterized using collimated-transmission absorption spectrophotometry in the same instrument. Optical measurements were made on phantoms composed of 75/25% v/v BBP/DEHA, 10% m/m PVC and containing 0 to 1% v/v BPC, 0 to 4 mg/mL TiO₂, or 0 to 200 mg/mL glass microspheres. Phantoms with glass microspheres only present very low-to-mild scattering over the concentrations studied, causing poor signal-to-noise ratio in spectrophotometry data. To improve the accuracy of calculated

optical properties, glass microsphere phantoms also contained a fixed concentration of 1.5 mg/mL TiO₂ to increase phantom turbidity. Optical absorption coefficient (μ_a) and reduced scattering coefficient (μ_s') spectra were calculated using the inverse adding-doubling (IAD) method,^{49,50} which requires knowledge of the anisotropy factor, g , and refractive index, n , of the sample. The refractive indices of BBP and DEHA are 1.540 and 1.447, respectively; using the Lorentz–Lorenz mixture rule for refractive index,⁵¹ 75/25% BBP/DEHA PVCP is expected to have a refractive index of 1.516. It is worth noting that the IAD's computed reduced scattering coefficient is relatively insensitive to the assumed value of g .⁴⁹ We assumed $g = 0.7$ based on Mie scattering theory for homogeneous spherical particles (using open-source MATLAB software⁵²). Calculation inputs include optical wavelength, particle refractive index (~ 2.5 for anatase TiO₂ in the near-infrared), background refractive index (1.516), and particle diameter (~ 550 nm, from dynamic light-scattering measurements of TiO₂ particles).

2.6 Temporal Stability

A high degree of mechanical durability and stability over time is necessary to ensure that image quality phantoms provide accurate, precise, and consistent estimates of image quality. To evaluate temporal stability, PVCP phantoms ($N = 8$) with similar geometry as above were made using 90/10% v/v BBP/DEHA, 10% m/m PVC, 1% v/v heat stabilizer, 1.4 mg/mL TiO₂, and 100 mg/mL silica particles (median diameter 10.5 μ m, MIN-U-SIL 40, U.S. Silica, Frederick, Maryland). Percent mass loss, optical properties, and acoustic properties were measured over 12 weeks. Initial phantom fabrication and mass measurements occurred 72 h prior to the first measurement time point. Phantoms were stored in a dry steel container at normal temperature and pressure.

2.7 Custom Photoacoustic Tomography System

To evaluate the use of PVCP phantoms for assessing PAT system performance, we developed a custom PAT system [Fig. 1(a)] comprised of a cart-based tunable near-infrared (NIR) pulsed laser/optical parametric oscillator (OPO) (Phocus Mobile, Opotek, Inc., Carlsbad, California) and a research-grade ultrasound system (Vantage 128, Verasonics, Kirkland, Washington) which provided a customizable MATLAB interface for instrument control. The OPO provided 5-ns laser pulses at repetition rates up to 10 Hz, over wavelengths from 690 to 950 nm, and at energies up to 120 mJ. Acoustic sensing was performed using a 128-channel ultrasound transducer array with a 7.5 MHz center frequency, 7.0 MHz bandwidth, and 38.1 mm length (L11-4v, Verasonics). The OPO sent a trigger signal to the ultrasound system to synchronize data acquisition per laser pulse. An engineered diffuser (ED1-L4100-MD, Thorlabs, Newton, New Jersey) was used to produce a 5 mm × 40 mm elliptical beam spot to ensure uniform illumination in the image plane. The optics assembly and transducer were affixed to a three-axis motorized translational stage for position control. Aluminum foil with a layer of acoustic coupling gel was fitted against the transducer surface to reduce reverberation artifacts due to high surface fluence and subsequent light absorption near the transducer. Image reconstruction was performed using a proprietary pixel-based reconstruction algorithm, and each frame was

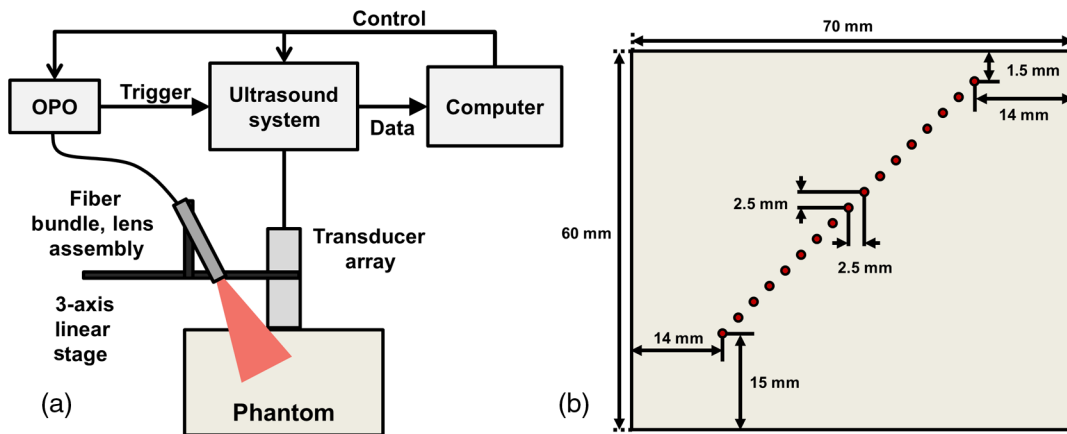


Fig. 1 (a) PAT system schematic and (b) PVCP fluid channel phantom geometry.

corrected for pulse–pulse energy variation using recordings from the OPO’s internal energy meter.

2.8 Image Quality Phantom

Simple image quality phantoms were constructed by pouring PVCP into a mold containing an array of 0.5 mm diameter steel wires spaced by 2.5 mm vertically and horizontally [Fig. 1(b)]. Due to the larger volume of these phantoms ($7 \times 7 \times 6 \text{ cm}^3$) compared with prior disk phantoms, the production method was scaled using a 250 mL flask and stronger stir bars. PVCP was poured in five sequential layers until the mold cavity was filled. After the PVCP cured, wires were extracted, leaving wall-less fluid channels that were injected with a well-controlled commercial oxyhemoglobin solution (Multi-4 CO-Oximeter Control, Instrumentation Laboratory, Bedford, Massachusetts). To compare our custom PVCP material with commercially available PVCP, two phantoms were constructed: (1) a custom PVCP phantom comprised of 75/25% v/v BBP/DEHA, 10% m/m PVC, 1.7 mg/mL TiO_2 , 50 mg/mL glass microspheres and (2) a commercial PVCP phantom containing 0.9 mg/mL TiO_2 , and 0.002% v/v BPC. These phantoms were designed to have the same optical properties, but different acoustic attenuation. This difference in acoustic attenuation was expected to affect penetration/visualization depth in the fluid channel array. Phantoms were imaged at 800 nm and radiant exposure of 20 mJ/cm^2 . PAT images were acquired at eight spatial locations along the transducer elevational axis, averaging 30 frames/location. Image data were normalized, log compressed, and displayed with eight-bit intensity mapping. Rectangular ROIs were selected around visually detectable targets for subsequent analysis. Because channels will appear as two spatially resolvable targets due to photoacoustic boundary buildup,⁵³ only ROI pixels above half the maximum ROI intensity were used for contrast calculations. Target contrast was calculated as the difference between the mean ROI intensity after masking by half the maximum ROI intensity and the mean local background intensity. To compare phantom performance results with real tissue conditions, imaging was also performed in a stack of either chicken breast muscle (pectoralis major) or pork loin chops (each slice was ~5- to 10-mm thick). A polytetrafluoroethylene tube containing oxyhemoglobin solution was placed between each slice in an array pattern similar to that in phantoms. Image

reconstruction in tissue experiments assumed a speed of sound of 1540 m/s.

3 Results and Discussion

3.1 Commercial Poly(vinyl chloride) Plastisol properties

Figure 2 shows the acoustic properties of commercial PVCP with added hardener. Hardener was found to significantly increase acoustic attenuation, but only produce small increases in speed of sound ($<1\%$). Additional hardener was also found to increase plastisol viscosity, making fabrication and uniform mixing more difficult. From these data, we can conclude that commercial PVCP, even with commercially available additives, does not possess adequately tunable acoustic properties for tissue phantoms.

A recent study reported speed of sound tunability from 1360 to 1580 m/s by varying hardener/base plastisol ratio in a commercial PVCP product based on DEHA.⁴⁴ However, we found that changing the resin content does not produce the reported degree of speed of sound tunability in commercial PVCP nor in custom PVCP formulations (see Sec. 3.3). Discrepancies may be due to differences in measurement techniques; our transmitter and receiver (centered near 7.5 MHz) were each mounted on five-dimensional stages (three linear axes and two angles) to ensure accurate transducer alignment. Our measurement system relied on radio-frequency signals, which are more accurate than ultrasound image signals for transit-time measurements because they contain phase information.

3.2 Liquid Plasticizer Properties

Table 2 shows speed of sound measured in 13 liquid plasticizers, as well as supplier-provided molecular weight and density data. The range of values was 1354 to 1540 m/s, which encompasses the range of values in most soft tissues, particularly fatty tissues. We also observed a positive correlation between speed of sound and plasticizer density, whereas no correlation was found with molecular weight. Of the four plasticizers selected for further characterization, three possessed high speed of sound values, while DEHA provided a much lower speed of sound. It is worth noting that DEHA is the

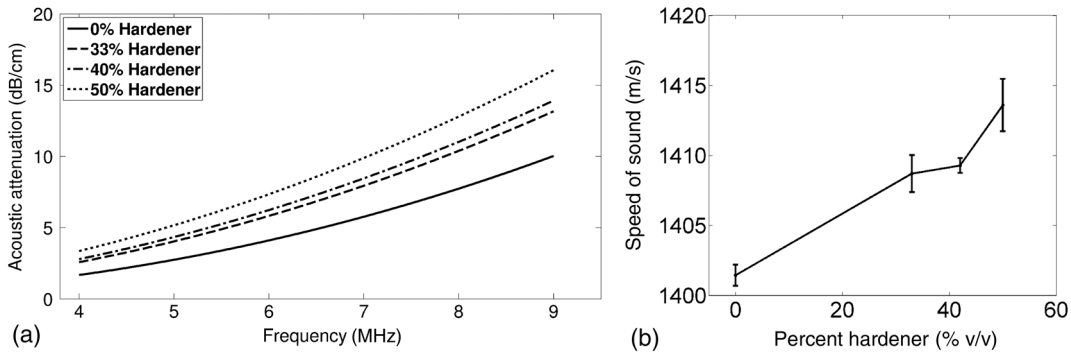


Fig. 2 (a) Acoustic attenuation and (b) speed of sound of commercial PVCP versus percent hardener. Error bars for attenuation data omitted for clarity, with coefficient of variation $\leq 1.7\%$. Error bars for speed of sound denote 95% confidence intervals.

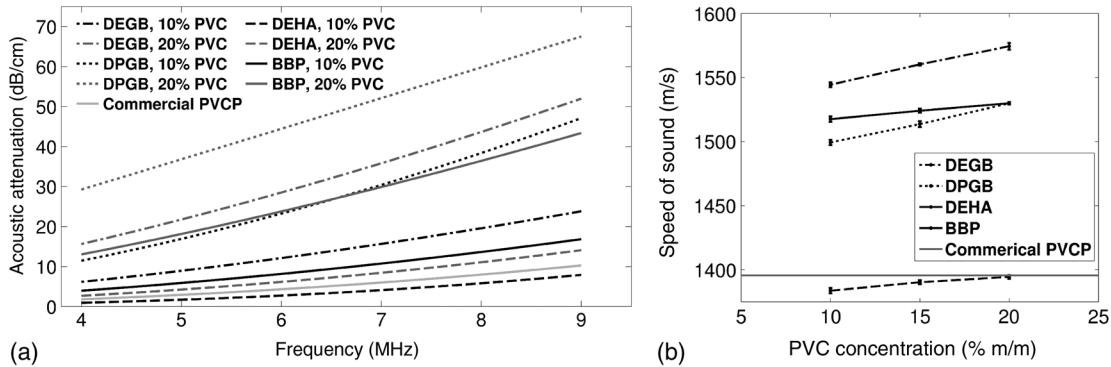


Fig. 3 (a) Acoustic attenuation versus PVC concentration in DPGB, DEGB, BBP, and DEHA gels as well as commercial PVCP gels. Attenuation data only shown for 10% and 20% PVC for clarity, and error bars are omitted for clarity, with coefficient of variation $\leq 3.6\%$. (b) Speed of sound versus PVC concentration and plasticizer type. Error bars for speed of sound denote 95% confidence intervals.

primary known plasticizer in the commercial PVCP used in this and other studies.^{37,38,44}

3.3 Acoustic Properties of Custom Poly(vinyl chloride) Plastisol Gels

The effect of PVC concentration on acoustic properties of single-plasticizer PVCP gels is shown in Fig. 3. Increased PVC concentration causes small increases in speed of sound, but substantial increases in acoustic attenuation. Choice of plasticizer also strongly influenced gel properties, with gel speed of sound closely following values measured in liquid plasticizers.

Speed of sound levels for PVCP gels are generally higher than those of the liquid plasticizers; this difference may be due to a combination of PVC having a higher intrinsic speed of sound and increased fusion and strengthening of the gel matrix due to higher PVC concentration. Differences in acoustic attenuation between gels may be due to differences in polymer-plasticizer solubility or affinity during the gelation and fusion processes. As shown in Fig. 4, speed of sound in PVCP gels containing binary mixtures of plasticizers may be tuned following a linear rule of mixtures, while acoustic attenuation follows a slightly nonlinear trend with plasticizer content and frequency. It is evident that DEGB and DPGB plasticizers produce PVCP with high

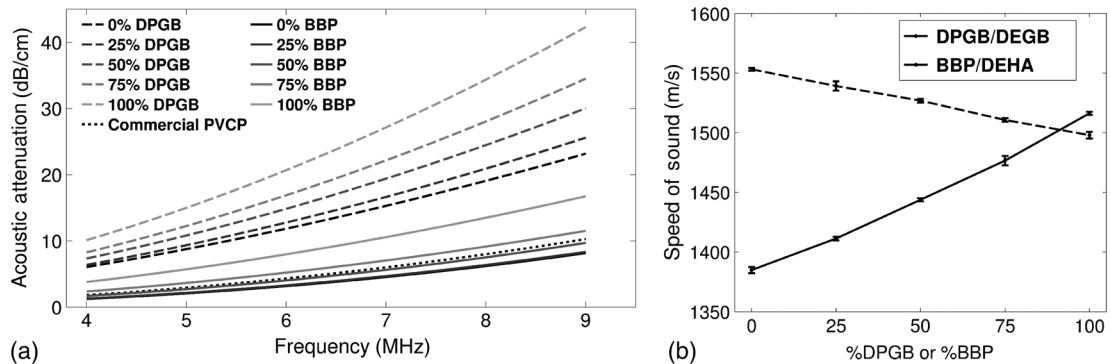


Fig. 4 (a) Acoustic attenuation and (b) speed of sound for DPGB/DEGB and BBP/DEHA PVCP gels. Error bars for attenuation data omitted for clarity, with coefficient of variation $\leq 5.8\%$. Error bars for speed of sound denote 95% confidence intervals.

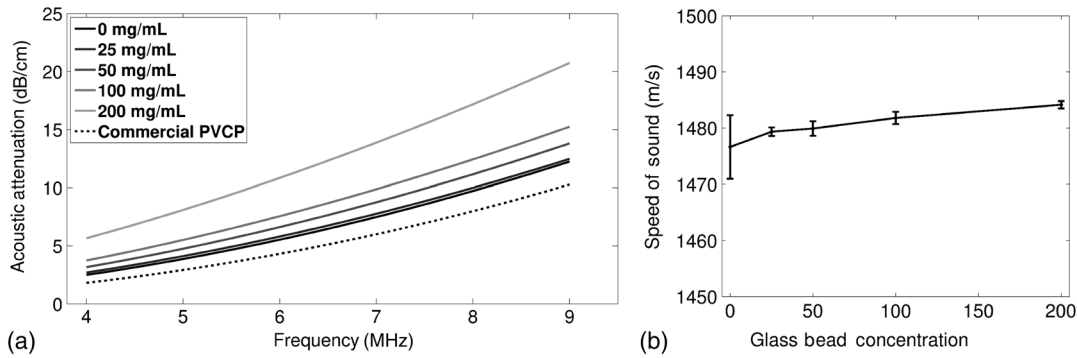


Fig. 5 (a) Acoustic attenuation and (b) speed of sound of 75/25% v/v BBP/DEHA, 10% m/m PVC gels versus glass microsphere concentration. Error bars for attenuation data omitted for clarity, with coefficient of variation $\leq 4.0\%$. Error bars for speed of sound denote 95% confidence intervals.

speed of sound, but also very high attenuation, while BBP/DEHA mixtures produce a broad tunable range for speed of sound with lower, more tissue-relevant attenuation. The speed of sound of the liquid heat stabilizer was measured as 1375 m/s; this value is similar to that of DEHA, and the low concentration (1% v/v) suggests a minimal impact on bulk properties.

Glass microspheres were shown to significantly increase acoustic attenuation (Fig. 5). Phantom attenuation exhibited an approximately linear frequency dependence due to the combined effect of acoustic absorption and scattering. At higher concentrations a slight increase in speed of sound may be seen, owing to the higher volume fraction occupied by the glass ($\sim 7\%$ at 200 mg/mL). Optical additives (BPC, TiO_2) did not significantly affect acoustic properties, which was expected given the low concentrations and small particle sizes of carbon black and TiO_2 (data not shown). Backscatter estimation results are shown in Fig. 6. Images shown in Figs. 6(a) and 6(b) were acquired using the same gain settings. Ultrasound images of PVCPC disks show bright horizontal bands at the contact surface with the reference phantom due to specular reflection. This feature allowed verification that ROIs were placed within the PVCPC disks. Mean ROI intensity depended linearly on glass microsphere concentration (up to at least 100 mg/mL), with a concentration of 50 mg/mL producing roughly equivalent intensity compared with the commercial reference breast

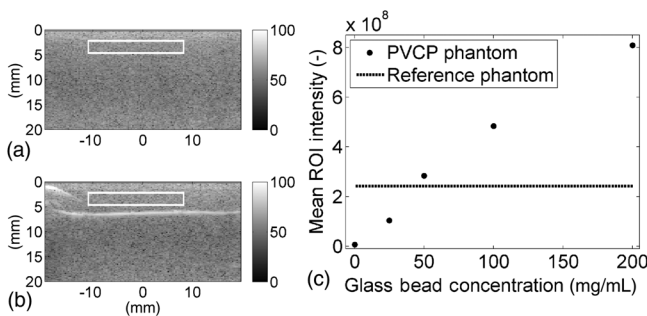


Fig. 6 Backscatter estimation of PVCPC samples with reference ultrasound phantom. Ultrasound images of (a) reference phantom and (b) reference phantom with PVCPC phantom disk containing 50 mg/mL glass microspheres on top. White box denotes analyzed ROI. (c) Mean ROI intensity versus PVCPC glass microsphere concentration.

phantom. In addition, the speckle pattern of the PVCPC disk resembled the speckle pattern of the commercial reference breast phantom. This suggests that PVCPC phantoms can be tuned to adequately approximate acoustic backscatter in soft tissues such as the breast, and may thus be suitable for bimodal ultrasound and photoacoustic imaging.

3.4 Optical Properties

Absorption spectra of the four liquid plasticizers are shown in Fig. 7. Absorption is generally flat between 600 and 800 nm, while varying peaks are present between ~ 850 to 1000 nm. Calculated optical properties in 75/25% v/v BBP/DEHA, 10% m/m PVC gels are shown in Figs. 8 and 9. BPC is capable of producing relatively flat absorption spectra with values similar to that of blood. Property values strongly overlap with the reported ranges for soft tissues (Table 1). The base PVCPC absorption spectrum at 0% BPC shows peaks in the NIR regime, which are characteristics of the plasticizers. As BPC content increases, these spectral peaks are minimized due to dominant BPC absorption. TiO_2 was found to produce high optical scattering, with decreasing scattering for longer wavelengths. Glass microspheres did not significantly affect scattering relative to added TiO_2 , but absorption was found to increase with glass microsphere concentration. However, at concentrations producing breast-relevant acoustic scattering (e.g., 50 mg/mL),

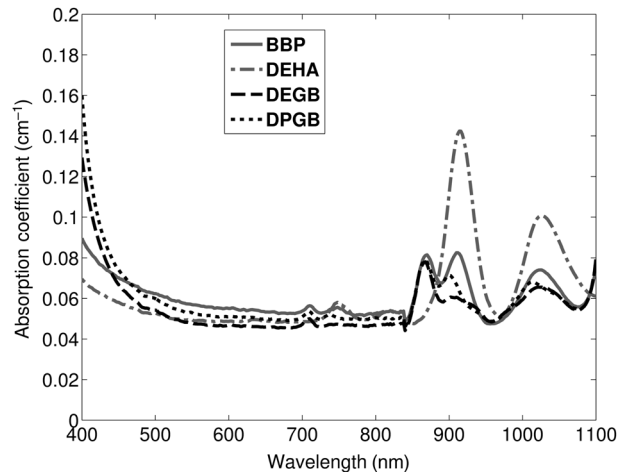


Fig. 7 Optical absorption spectra of liquid plasticizers.

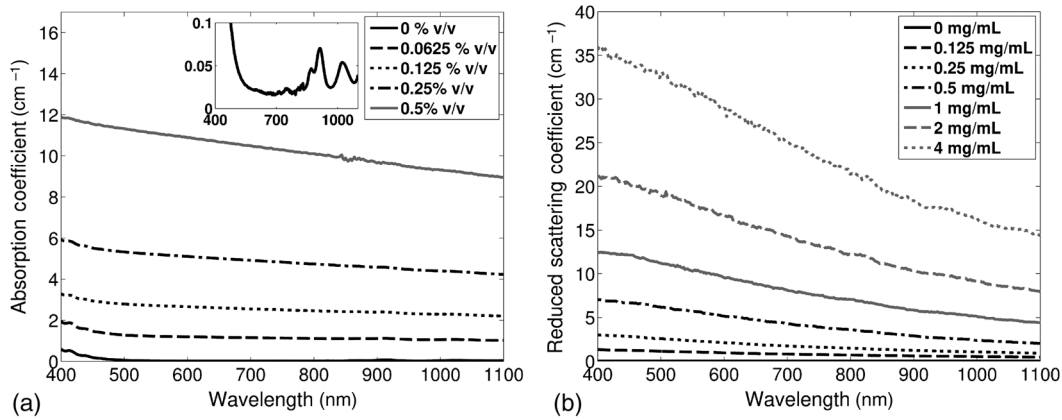


Fig. 8 Optical properties of phantoms comprised of 75/25% v/v BBP/DEHA, 10% m/m PVC. (a) Optical absorption coefficient versus % v/v BPC. Inset shows the 0% v/v spectrum, with axes in similar units. (b) Reduced scattering coefficient versus TiO_2 concentration.

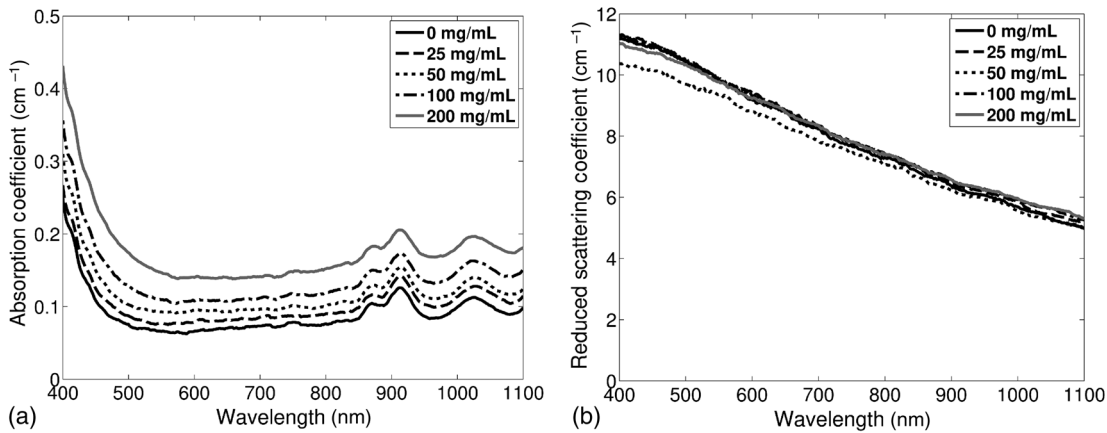


Fig. 9 (a) Optical absorption and (b) reduced scattering coefficients versus glass microsphere concentration in 75/25% v/v BBP/DEHA, 10% m/m PVC gels.

the absorption coefficient is still breast-relevant at $\sim 0.1 \text{ cm}^{-1}$. The negligible scattering is expected because of the high refractive index matching between PVCP (1.516) and glass microspheres (~ 1.50 to 1.55).

Optical absorption and scattering dopants were characterized only in a single PVCP formulation. Because PVCP with different plasticizer ratios will have different bulk refractive indices, the index mismatch (thus, scattering strength) of TiO_2 particles will depend on PVCP composition. As such, calibration curves for optical dopant concentration should be determined for a given base PVCP composition. Additionally, the viscosity of PVCP solution (both before and after heating) varies with plasticizer and resin content. While we did not experience issues with dopant miscibility or suspension quality in the formulations used in this study, very high viscosities may result in inadequate TiO_2 sonication, which would affect the scattering concentration curve. In general, TiO_2 suspension quality in PVCP is sufficient to produce scattering over the entire range of biologically relevant values.

3.5 Material Stability

Stability results for BBP/DEHA phantoms are shown in Fig. 10. Small mass losses occur over time, but no monotonic trends are

observed in measured acoustic properties. Mean optical absorption and reduced scattering coefficients appear to decrease at 8 weeks, but this trend was not found to be statistically significant. This variation between time points is likely due in part to experimental precision, rather than transient material changes. PVCP gels will be slightly deformed when measured with calipers or lightly held between glass slides, changing sample thickness from its nominal value. Varying the IAD sample thickness value input $\pm 0.2 \text{ mm}$ ($\pm 4\%$) caused estimated absorption and scattering outputs to vary by up to $\pm 8\%$, while mean optical properties changed by up to 10% over 12 weeks. The combination of precision error and statistical error suggests that phantom optical properties are stable over at least 12 weeks.

The probable mass loss mechanism is volatile losses, i.e., a combination of surface evaporation and plasticizer exudation/porous diffusion. We chose to store phantoms in air at normal temperature and pressure as a conservative estimate of phantom shelf life under typical usage conditions. In a more robustly fabricated image quality phantom, the phantom could be encased in a solid chamber and sealed with a thin plastic membrane to prevent environmental exposure and increase shelf life. Also, the relatively small size of these phantoms results in a higher surface-area-to-volume ratio, which may increase volatile losses compared with a larger phantom.⁵⁴ We have observed

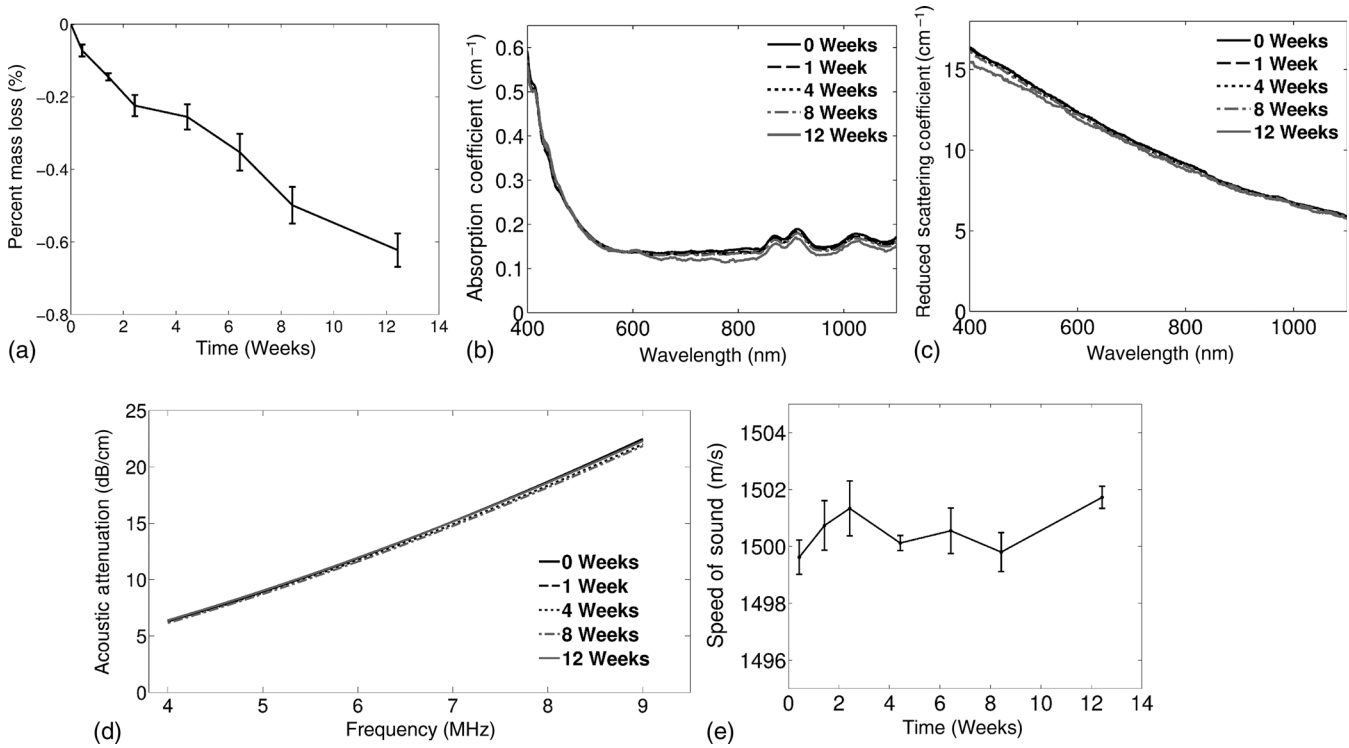


Fig. 10 PVC gel properties over a period of 12 weeks, including (a) mass loss, (b) optical absorption, (c) optical scattering, (d) acoustic attenuation, and (e) speed of sound. Curves in (b)–(d) are mean spectra with error bars omitted for clarity. Error bars in (a) and (e) denote 95% confidence intervals. Coefficients of variation were (b) $\leq 6.8\%$, (c) $\leq 2.7\%$, and (d) $\leq 3.0\%$.

that storage at lower temperatures can reduce plasticizer exudation, but storage below 0°C can cause permanent damage. We have also qualitatively observed that temporal stability may increase with PVC resin concentration, but this could be undesirable depending on acoustic property requirements.

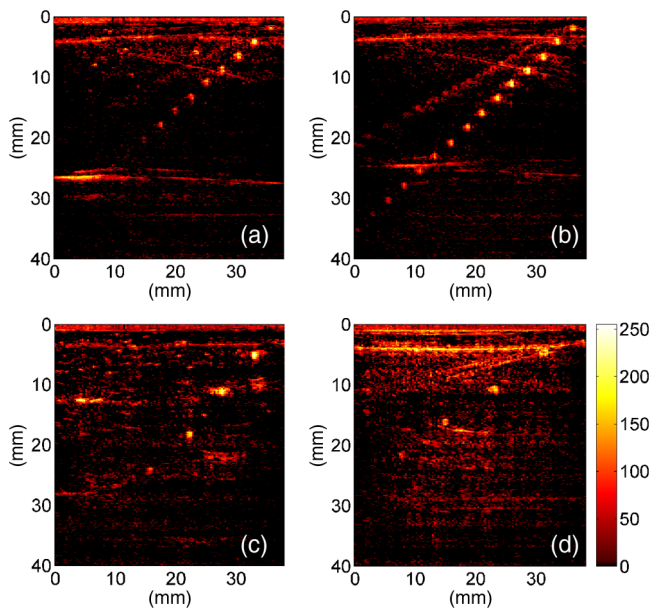


Fig. 11 Representative photoacoustic images in (a) custom PVC phantom, (b) commercial PVC phantom, (c) chicken tissue, and (d) porcine tissue.

3.6 Imaging Results

As shown in Fig. 11, phantom images generally presented high background before background subtraction as well as near-field clutter due to both high surface fluence and streak artifacts caused by small ridges in the aluminum foil. Additionally, shallow targets produce reconstruction artifacts that appear as streaks extending laterally into deeper phantom regions. The combination of these artifacts and high near-field clutter resulted in lower contrast for shallow targets. As shown in Fig. 12, measured penetration depth is significantly lower in the custom breast-simulating PVC phantom versus the commercial PVC phantom, at ~ 23 mm versus ~ 32 mm, respectively (based on qualitative limit of detectability). Because phantom optical attenuation is well-matched [Fig. 12(a)], penetration differences must be due to higher acoustic attenuation in the BBP/DEHA phantom. Additionally, higher acoustic attenuation also appears to mitigate shallow reconstruction artifacts in BBP/DEHA phantoms. Penetration depth in chicken breast and porcine tissue was similar to that observed in both custom and commercial PVC phantoms, demonstrating that both phantoms produce biologically relevant PAT system performance. However, penetration in porcine tissue was lower than that in chicken tissue, which is consistent with preliminary acoustic property measurements (at 7.5 MHz, $\alpha_{\text{chicken}} \sim 4$ dB/cm, $\alpha_{\text{porcine}} \sim 8$ dB/cm). These results indicate that our custom formulation is a better tissue analog than commercial PVC when the intended application involves tissues with higher acoustic attenuation (e.g., breast). These results illustrate the impact of tunable phantom acoustic properties on image quality testing and performance metrics.

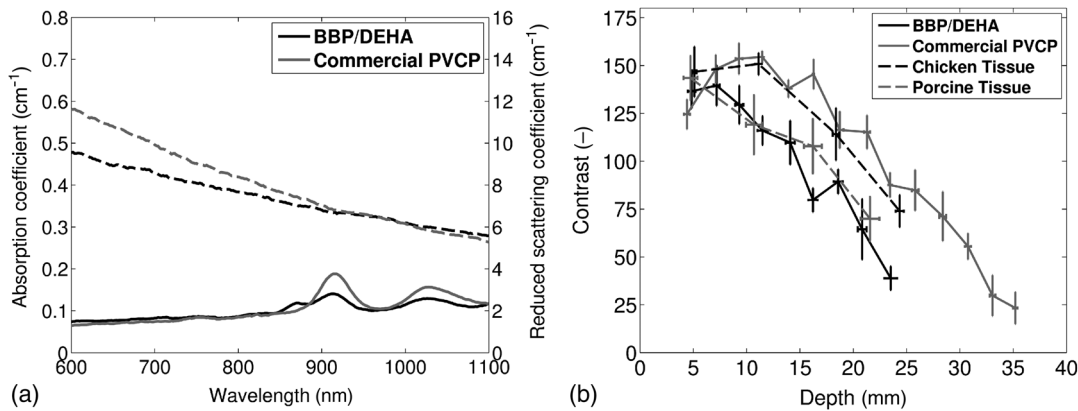


Fig. 12 (a) Absorption (solid lines) and reduced scattering (dashed lines) coefficients of the two phantoms. (b) Contrast versus depth in phantoms and tissue experiments. Error bars denote ± 1 standard deviation.

4 Conclusion

We have designed and characterized a stable customizable PVC plastisol formulation with tunable optical and acoustic properties, and used this material to produce breast-relevant phantoms suitable for evaluating photoacoustic imaging system performance. Future work will focus on optimization of plastisol formulations and development of comprehensive phantom-based performance test methods for photoacoustic imaging systems.

Acknowledgments

The authors gratefully acknowledge funding support from the FDA Medical Countermeasures Initiative and the FDA Office of Women's Health, as well as the ORISE fellowship program through Oak Ridge Associated Universities. The authors also wish to thank Irada Isayeva, Ph.D., and Katherine Vorvolakos, Ph.D., of the Center for Devices and Radiological Health for insightful discussions.

References

- L. H. V. Wang and S. Hu, "Photoacoustic tomography: in vivo imaging from organelles to organs," *Science* **335**(6075), 1458–1462 (2012).
- T. N. Erpelding et al., "Sentinel lymph nodes in the rat: noninvasive photoacoustic and US imaging with a clinical US system," *Radiology* **256**(1), 102–110 (2010).
- C. Kim et al., "Deeply penetrating in vivo photoacoustic imaging using a clinical ultrasound array system," *Biomed. Opt. Express* **1**(1), 278–284 (2010).
- L. S. Bouchard et al., "Picomolar sensitivity MRI and photoacoustic imaging of cobalt nanoparticles," *Proc. Natl. Acad. Sci. U. S. A.* **106**(11), 4085–4089 (2009).
- J. Laufer et al., "In vitro measurements of absolute blood oxygen saturation using pulsed near-infrared photoacoustic spectroscopy: accuracy and resolution," *Phys. Med. Biol.* **50**(18), 4409–4428 (2005).
- R. A. Kruger et al., "Photoacoustic angiography of the breast," *Med. Phys.* **37**(11), 6096–6100 (2010).
- IEC 61391.1:2006, "Ultrasonics—pulse-echo scanners—part 1: techniques for calibrating spatial measurement systems and measurement of system point-spread function response," IEC, Geneva, Switzerland.
- IEC 61391-2:2006, "Ultrasonics—pulse-echo scanners—part 2: measurement of maximum depth of penetration and local dynamic range," IEC, Geneva, Switzerland.
- C. H. McCollough et al., "The phantom portion of the American College of Radiology (ACR) computed tomography (CT) accreditation program: practical tips, artifact examples, and pitfalls to avoid," *Med. Phys.* **31**(9), 2423–2442 (2004).

- ACR, "Phantom test guidance for the ACR MRI accreditation program," American College of Radiology, (2005), <http://www.acr.org/quality-safety/accreditation/mri> (10 January 2015).
- B. W. Pogue and M. S. Patterson, "Review of tissue simulating phantoms for optical spectroscopy, imaging and dosimetry," *J. Biomed. Opt.* **11**(4), 041102 (2006).
- G. Lamouche et al., "Review of tissue simulating phantoms with controllable optical, mechanical and structural properties for use in optical coherence tomography," *Biomed. Opt. Express* **3**(6), 1381–1398 (2012).
- N. Bosschaart et al., "A literature review and novel theoretical approach on the optical properties of whole blood," *Lasers Med. Sci.* **29**, 453–479 (2014).
- F. A. Duck, *Physical Properties of Tissue*, Academic Press, London (1990).
- J. L. Sandell and T. C. Zhu, "A review of in vivo optical properties of human tissues and its impact on PDT," *J. Biophotonics* **4**(11–12), 773–787 (2011).
- P. D. Edmonds et al., "Ultrasound tissue characterization of breast biopsy specimens," *Ultrason. Imaging* **13**(2), 162–185 (1991).
- W. F. Xia et al., "Design and evaluation of a laboratory prototype system for 3D photoacoustic full breast tomography," *Biomed. Opt. Express* **4**(11), 2555–2569 (2013).
- S. Manohar et al., "Photoacoustic mammography laboratory prototype: imaging of breast tissue phantoms," *J. Biomed. Opt.* **9**(6), 1172–1181 (2004).
- S. Manohar et al., "The Twente photoacoustic mammoscope: system overview and performance," *Phys. Med. Biol.* **50**(11), 2543–2557 (2005).
- M. Heijblom et al., "Imaging tumor vascularization for detection and diagnosis of breast cancer," *Technol. Cancer Res. T* **10**(6), 607–623 (2011).
- S. A. Ermilov et al., "Laser optoacoustic imaging system for detection of breast cancer," *J. Biomed. Opt.* **14**(2), 024007 (2009).
- F. T. D'Astous and F. S. Foster, "Frequency-dependence of ultrasound attenuation and backscatter in breast-tissue," *Ultrasound Med. Biol.* **12**(10), 795–808 (1986).
- I. Katz-Hanani et al., "Age-related ultrasonic properties of breast tissue in vivo," *Ultrasound Med. Biol.* **40**(9), 2265–2271 (2014).
- K. Zell et al., "Acoustical properties of selected tissue phantom materials for ultrasound imaging," *Phys. Med. Biol.* **52**(20), N475–N484 (2007).
- C. Avigo et al., "Organosilicon phantom for photoacoustic imaging," *J. Biomed. Opt.* **20**(4), 046008 (2015).
- J. Laufer, E. Zhang, and P. Beard, "Evaluation of absorbing chromophores used in tissue phantoms for quantitative photoacoustic spectroscopy and imaging," *IEEE J. Sel. Top. Quant.* **16**(3), 600–607 (2010).
- S. L. Vieira et al., "Paraffin-gel tissue-mimicking material for ultrasound-guided needle biopsy phantom," *Ultrasound Med. Biol.* **39**(12), 2477–2484 (2013).

28. M. Wang et al., "3D printing method for freeform fabrication of optical phantoms simulating heterogeneous biological tissue," *Proc. SPIE* **8945**, 894509 (2014).
29. J. R. Cook, R. R. Bouchard, and S. Y. Emelianov, "Tissue-mimicking phantoms for photoacoustic and ultrasonic imaging," *Biomed. Opt. Express* **2**(11), 3193–3206 (2011).
30. W. F. Xia et al., "Poly(vinyl alcohol) gels as photoacoustic breast phantoms revisited," *J. Biomed. Opt.* **16**(7), 075002 (2011).
31. A. Dima and V. Ntziachristos, "Non-invasive carotid imaging using optoacoustic tomography," *Opt. Express* **20**(22), 25044–25057 (2012).
32. P. Ephrat et al., "Localization of spherical lesions in tumor-mimicking phantoms by 3D sparse array photoacoustic imaging," *Med. Phys.* **37**(4), 1619–1628 (2010).
33. Z. Xu, C. H. Li, and L. V. Wang, "Photoacoustic tomography of water in phantoms and tissue," *J. Biomed. Opt.* **15**(3), 036019 (2010).
34. J. Su et al., "Photoacoustic imaging of clinical metal needles in tissue," *J. Biomed. Opt.* **15**(2), 021309 (2010).
35. A. Kharine et al., "Poly(vinyl alcohol) gels for use as tissue phantoms in photoacoustic mammography," *Phys. Med. Biol.* **48**(3), 357–370 (2003).
36. C. Haisch et al., "Combined optoacoustic/ultrasound system for tomographic absorption measurements: possibilities and limitations," *Anal. Bioanal. Chem.* **397**(4), 1503–1510 (2010).
37. G. M. Spirou et al., "Optical and acoustic properties at 1064 nm of polyvinyl chloride-plastisol for use as a tissue phantom in biomedical photoacoustics," *Phys. Med. Biol.* **50**(14), N141–N153 (2005).
38. S. E. Bohndiek et al., "Development and application of stable phantoms for the evaluation of photoacoustic imaging instruments," *Plos One* **8**(9), e75533 (2013).
39. B. Lashkari and A. Mandelis, "Comparison between pulsed laser and frequency-domain photoacoustic modalities: Signal-to-noise ratio, contrast, resolution, and maximum depth detectivity," *Rev. Sci. Instrum.* **82**(9), 094903 (2011).
40. W. Lu et al., "Photoacoustic imaging of living mouse brain vasculature using hollow gold nanospheres," *Biomaterials* **31**(9), 2617–2626 (2010).
41. B. Tavakoli and Q. Zhu, "Depth-correction algorithm that improves optical quantification of large breast lesions imaged by diffuse optical tomography," *J. Biomed. Opt.* **16**(5), 056002 (2011).
42. S. Telenkov et al., "Frequency-domain photoacoustic phased array probe for biomedical imaging applications," *Opt. Lett.* **36**(23), 4560–4562 (2011).
43. M. Fonseca et al., "Characterisation of a PVCP based tissue-mimicking phantom for quantitative photoacoustic imaging," *Proc SPIE* **9539**, 953911 (2015).
44. N. Hungr et al., "A realistic deformable prostate phantom for multimodal imaging and needle-insertion procedures," *Med. Phys.* **39**(4), 2031–2041 (2012).
45. A. C. Shah and D. J. Poledna, "Review of PVC dispersion and blending resin products," *J. Vinyl. Add. Technol.* **9**(3), 146–154 (2003).
46. M. O. Culjat et al., "A review of tissue substitutes for ultrasound imaging," *Ultrasound Med. Biol.* **36**(6), 861–873 (2010).
47. K. A. Wear, "Cancellous bone analysis with modified least squares Prony's method and chirp filter: Phantom experiments and simulation," *J. Acoust. Soc. Am.* **128**(4), 2191–2203 (2010).
48. K. A. Wear, "Measurements of phase velocity and group velocity in human calcaneus," *Ultrasound Med. Biol.* **26**(4), 641–646 (2000).
49. S. A. Prahl, M. J. C. Van Gemert, and A. J. Welch, "Determining the optical-properties of turbid media by using the adding-doubling method," *Appl. Opt.* **32**(4), 559–568 (1993).
50. S. A. Prahl, "Inverse adding-doubling," (2007), <http://omlc.org/software/iad/> (10 January 2015).
51. W. Heller, "Remarks on refractive index mixture rules," *J. Phys. Chem.* **69**(4), 1123–1129 (1965).
52. S. A. Prahl, "Mie scattering," (2012), <http://omlc.org/software/mie/> (10 January 2015).
53. A. Q. Bauer et al., "Quantitative photoacoustic imaging: correcting for heterogeneous light fluence distributions using diffuse optical tomography," *J. Biomed. Opt.* **16**(9), 096016 (2011).
54. R. F. Grossman, *Handbook of Vinyl Formulating*, 2nd ed., John Wiley & Sons, Inc., New Jersey (2008).

William C. Vogt received his BS degree in mechanical engineering from the University of Massachusetts Amherst in 2009 and his PhD in biomedical engineering from Virginia Polytechnic Institute and State University in 2013. Since 2013, he has been conducting photoacoustic imaging research as a research fellow at the FDA in the Office of Science and Engineering Laboratories. His research interests include photoacoustic imaging, phantom-based image quality testing, and biophotonic medical device characterization and evaluation.

Congxian Jia received her BS and MS degrees in mechanical engineering from Beijing University, China, in 1999 and 2002, respectively. She also received her MS degree in biomechanics of aerospace and mechanical engineering from Boston University in 2004 and the PhD in biomedical engineering from the University of Michigan in 2010. Currently, she works as a research fellow at the FDA, and her research interests include ultrasound elasticity imaging and photoacoustic imaging.

Keith A. Wear received his MS and PhD degrees in applied physics from Stanford University in 1982 and 1987, respectively. Since 1989, he has worked at the FDA. He is an associate editor of three journals: *Journal of the Acoustical Society of America*, *IEEE Transactions on Ultrasonics, Ferroelectrics, and Frequency Control*, and *Ultrasonic Imaging*. He is a fellow of the Acoustical Society of America, the American Institute for Medical and Biological Engineering, and the American Institute of Ultrasound in Medicine.

Brian S. Garra trained at the University of Washington and the University of Utah and currently practices radiology at the Washington DC Veterans Affairs Medical Center. He also does research and medical device evaluation at the FDA as an associate director-clinical in the Division of Imaging, Diagnostics and Software Reliability. Currently, he is working on elastography, phantoms for photoacoustic system/elastographic system evaluation, the quantitative imaging biomarker alliance (QIBA), and ultrasound outreach in Peru.

T. Joshua Pfefer received his BS degree in mechanical engineering from Northwestern University, his MS degree in mechanical engineering, and his PhD in biomedical engineering from the University of Texas at Austin, and was a research fellow at the Wellman Laboratories of Photomedicine. In 2000, he joined the FDA, where he is currently the leader of the Optical Diagnostic Devices Laboratory. His group's research focuses on safety and effectiveness in emerging clinical biophotonic spectroscopy and imaging technologies.